IEEE Photonics Journal
An IEEE Photonics Society Publication

Open Access

Double Anticrossing Coupling in a Single Metal-Clad Microcapillary

Volume 10, Number 3, June 2018

Yu Xiang
Yuejiang Song

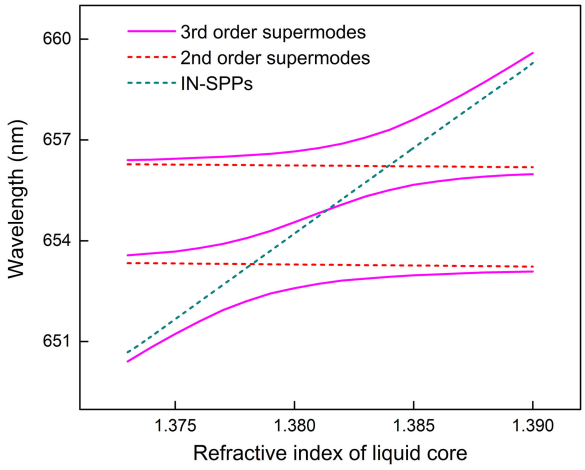

DOI: 10.1109/JPHOT.2018.2830652
1943-0655 © 2018 IEEE

IEEE photonics SOCIETY

IEEE

Double Anticrossing Coupling in a Single Metal-Clad Microcapillary

Yu Xiang and Yuejiang Song

College of Engineering and Applied Science, Nanjing University, Nanjing 210093, China

DOI:10.1109/JPHOT.2018.2830652

Manuscript received March 24, 2018; revised April 19, 2018; accepted April 22, 2018. Date of publication April 27, 2018; date of current version May 18, 2018. This work was supported by the National Science Foundation of China under Grant 60907022. Corresponding author: Yuejiang Song (e-mail: yjsong@nju.edu.cn).

Abstract: Mode coupling is studied comprehensively in a proposed metal-clad microcapillary cavity, which is an optofluidic capillary with two silver films coated on both surfaces of the silica wall. The dispersion relations of resonant wavelength dependencies on wall thickness of silica microcapillary and surrounding medium index are calculated, and different types of mode coupling are observed clearly. Besides the reported traditional mode coupling, double anticrossing coupling involving two plasmonic modes and one photonic mode is achieved in a single cavity for the first time. Also, *Q* factors and field distributions of coupled modes are calculated, manifesting that the coupled modes are the high *Q* factor hybrid modes. The field evolutions of coupled modes are interpreted well by the effective potential approach. The coupled modes in such a metal-clad microcapillary could find some interesting applications requiring both the high *Q* factor and the high field enhancement factor.

Index Terms: Microcavity, surface plasmon polariton (SPP), whispering gallery mode (WGM), mode coupling.

1. Introduction

Optical whispering gallery microcavities with small mode volume and ultrahigh quality factor have gained considerable interests in recent decades [1]–[3], leading to many important applications including low threshold laser [4], [5], high resolution biochemical sensor [4], [6] and on-chip integration [7], [8]. At the same time a variety of plasmonic resonators were proposed and studied intensively to achieve plasmonic resonance with ultrasmall mode volume, but quite low Q factor [9], [10]. However, metal coated microcavities, with metal film coated on the surface of dielectric microcavities, could bring about the interaction of WG modes and surface plasmonic modes, resulting in high quality factor hybrid photon-plasmon modes, when these modes have the approximate effective mode indices [11]–[14]. Until now, only single anti-crossing coupling between two modes, one plasmonic mode and one WG mode, has been observed and investigated in metal coated microspheres [15] and plasmonic microbubbles [16]. Such a mode coupling in the metal coated microcavity is due to that plasmonic mode has a special dispersion curve opposite to photonic modes. The supermode combining plasmonic mode and photonic mode possesses both high Q factor and high field enhancement factor, which makes it potential for many interesting applications requiring both high Q factor and field enhancement factor, such as biochemical sensor and nonlinear effect. But strong double anti-crossing coupling has not been reported in a single cavity, which is, however,

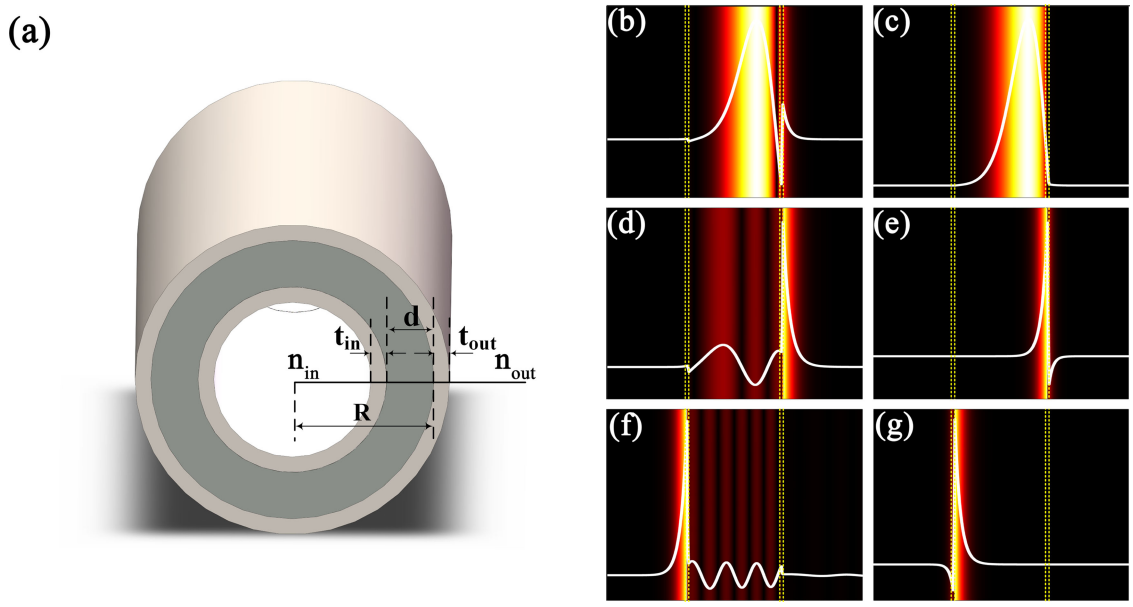

Fig. 1. (a) Schematic illustration of a metal-clad microcapillary. Two silver films are coated on the inner and outer surfaces of the dielectric microcapillary. The EM field distributions of typical resonant modes: (b) TM1 mode, (c) TE1 mode, (d) EX-SPPs mode, (e) EX-SPPa mode, (f) IN-SPPs mode, and (g) IN-SPPa mode in MCM.

of importance for the understanding the evolution of photon-plasmon modes in a plasmonic cavity and many interesting applications.

Here, in this paper, we will study comprehensively all different kinds of photonic/plasmonic mode coupling, especially plasmonic/photonic/plasmonic three-mode coupling, in a single metal-clad microcapillary (MCM), which is the microcylinder cavity with two metal films coated on both surfaces of silica microcapillary. In this cavity, photonic modes can be supported in microcapillary wall, and plasmonic modes can be generated on the surfaces of two metal films. The dispersion curves of resonant wavelength dependences of different modes on wall thickness of silica microcapillary and surrounding medium index are calculated for this MCM cavity. In the dispersion curves, different types of mode coupling can be observed clearly, and all these mode couplings are due to abnormal dispersion property of plasmonic mode, totally opposite to the photonic modes. Besides the low order two-mode coupling reported before, high order plasmonic/photonic/plasmonic three-mode coupling is observed for the first time, where two SPP modes and one photonic mode are involved. This high order coupled mode can have more advantages than low order coupled mode, such as more power fraction on the cavity surfaces, which may bring stronger light-matter interaction. Also, the field distributions and Q factors of two different coupled modes are calculated simultaneously, manifesting that the coupled modes are the high Q factor hybrid plasmonic/photonic modes. And the field evolution of coupled mode is interpreted well by an effective potential approach. Above all, arbitrary manipulation of strong coupling between plasmonic modes and photonic modes pave a way for the study of enhanced light-matter interactions and potential sensing applications.

2. Proposed MCM Structure

The proposed plasmonic MCM is shown in Fig. 1(a). It consists of a silica microcapillary and two silver films coated on the inner and outer surfaces of the microcapillary. R and d are the outer radius and wall thickness of silica microcapillary, t_{in} and t_{out} are the thicknesses of inner and outer metal films, respectively. MCM is surrounded by the inner and outer dielectric media, and the refractive indices of these inner and outer media are denoted as n_{in} and n_{out} respectively. In the following

study, t_{in} and t_{out} are both fixed at 60 nm, R is set as 71.2 μm, which doesn't lose the research generality. At room temperature, the permittivities of silica and silver are $\varepsilon_1 = 1.4565^2$ [17] and $\varepsilon_2 = (0.052225 + 4.4094\ i)^2$ [18] in the 650 nm band, respectively. The parameters d, n_{in} and n_{out} can be varied to investigate the modal evolutions.

3. Results and Discussions

Firstly, we present the typical modes that are far away from strong mode coupling in MCMs. In this paper, Finite Element Method (COMSOL Multiphysics 3.5a) is used to simulate the mode properties, such as resonant wavelengths, Q factors and field distributions of different modes in the proposed cavity [19]. Fig. 1(b)–(g) show field intensity distributions of the typical modes in a specific MCM, of which silica wall thickness d is fixed at 3.5 μm and the refractive indices of both inner and outer media are the same 1.33. Their radial field profiles in white lines are overlaid on Fig. 1(b)–(g). As shown in Fig. 1(b), TM1 mode in a MCM is actually a weakly hybrid plasmon-photon mode in the metal-clad microcavity. For these TM modes, their most energy is confined in the silica wall, and only little energy is localized near the surfaces of metal film (the outer metal film shown in Fig. 1(a)). By contrast, in Fig. 1(c), TE1 mode has almost no energy near the metal film surfaces, which is similar to TE1 mode in pure dielectric microcapillary. In this paper, TM and TE modes are characterized by an optical electric field perpendicular and parallel to the microcapillary axis, respectively. Fig. 1(d) and (e) are two types of SPP modes, symmetric mode (SPPs mode) and asymmetric mode (SPPa mode), localized near the two surfaces of the outer metal film. We name these two plasmonic modes as EX-SPPs mode and EX-SPPa mode respectively. The prefix EX denotes that the mode is localized on an outer metal film. EX-SPPs mode has the same sign of amplitude on both surfaces of the metal film, so it is named as a symmetric mode. Similarly, EX-SPPa mode has the opposite signs of amplitude on two sides of the metal film, so named as an asymmetric mode. The peak amplitude of EX-SPPs mode is on the outer surface, while that of EX-SPPa mode is on the inner surface, these two SPP modes have inherently different properties, especially on their dispersion curves or effective indices [15]. Similarly the modes shown in Fig. 1(f) and (g) are the plasmonic modes, IN-SPPs mode and IN-SPPa mode, localized on the inner metal film.

Next, to better understand the modal evolutions in MCMs, we now investigate the modal dispersion relations and field spatial distributions. Here the inner and outer surrounding media have the same index of 1.33 and the wall thickness d is varied from 0.8 μm to 3.5 μm. In all the below calculations, only SPPs modes and TM modes are considered because these two kinds of resonant modes can couple with each other in our calculated range. And SPPa modes and TE modes are omitted. The resonant wavelength dependences of TM modes and SPPs modes (azimuthal mode number $M = 956$) on silica wall thickness d is plotted in Fig. 2(a). As shown in Fig. 2(a), outside of mode coupling (drawn in red lines), the resonant wavelengths of TM modes increase with wall thickness d, showing a normal dispersion. For example, TM2 mode is firstly generated at its threshold wall thickness of $\sim$1.1 μm. Its resonant wavelength increases quickly with d from $\sim$1.1 μm to $\sim$2.2 μm, then increases slowly and finally keeps almost constant with d greater than $\sim$2.8 μm. This is because the resonant wavelength is mainly affected by wall thickness d for a thin wall microcavity, but by outer diameter (fixed in our calculation) for a thick wall microcavity. This can be well explained by effective potential approach [20]. But opposite to TM modes, the resonant wavelength of IN-SPPs plasmonic mode decreases almost linearly with d and that of EX-SPPs mode keeps nearly constant, showing an abnormal dispersion. This is due to that the resonant wavelengths of two SPPs plasmonic modes are nearly linear with the radii of metal films, fixed outer radius ($R + t_{out}$) of outer metal film for EX-SPPs mode and variable inner radius ($R - d - t_{in}$) of inner metal film for IN-SPPs mode. Moreover, most important of all, many anti-crossing couplings between EX- or IN-SPPs modes and TM modes are achieved and highlighted in Fig. 2(a) with red lines when these modes have approximately equal resonant wavelengths. Due to their different dispersion properties, the dispersion curve of SPPs mode can meet with that of TM modes at an appropriate

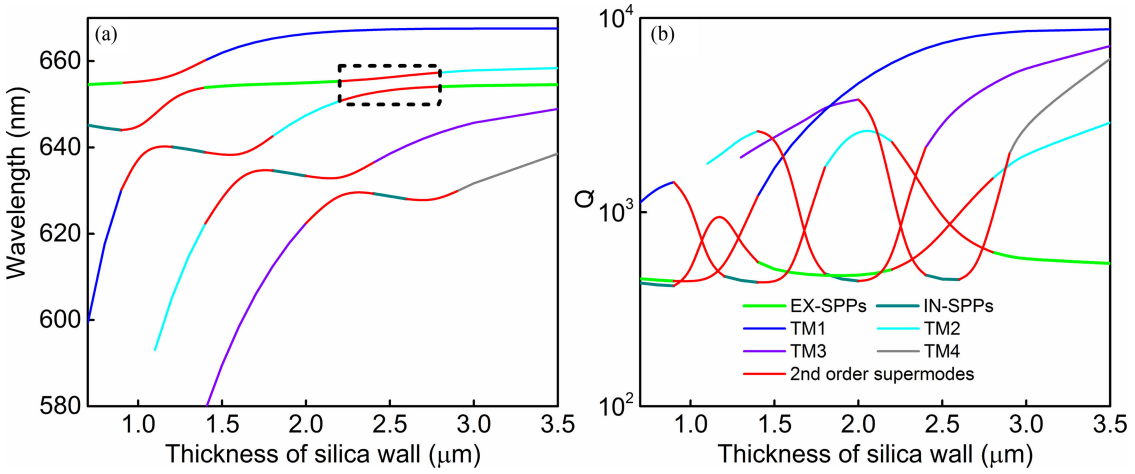

Fig. 2. (a) Resonant wavelength and (b) Q factor dependences of different modes (azimuthal mode number $M = 956$) in MCMs on the thickness of silica wall d.

d. As shown in Fig. 2(a), EX-SPPs (green line) couples with TM1 and TM2 modes successively when d is around 1.3 μm and 2.5 μm. IN-SPPs mode (dark cyan line) couples with TM1, TM2 and TM3 modes successively when d is at the proximity of 1.1 μm, 1.7 μm and 2.2 μm. Such the mode couplings will produce hybrid plasmonic/photonic modes or 2nd order supermodes involving two fundamental modes. Q factors and field distributions of these supermodes will be discussed in detail below. In Fig. 2(a), both IN- and EX-SPPs mode couple with higher order TM4 mode can be predicted well. Actually, EX-SPPs, TM1 and IN-SPPs modes couple with each other to produce double anti-crossing when d is around 1.2 μm. Double anti-crossing coupling will be discussed in detail below.

Meanwhile, Q factors of SPPs modes and TM modes are depicted in Fig. 2(b). Outside of coupling region, Q factors of photonic modes increase to nearly 10^4 with the increase of d, and are much larger than those of SPPs modes. Successive crossings of Q factor indicate that EX-SPPs or IN-SPPs mode strongly couples with different photonic modes in sequence with the increase of d. In coupling range, Q factors of these supermodes change dramatically due to intense energy exchange between photonic modes and plasmonic modes. And their Q factors are enhanced greatly due to mode coupling, compared with pure plasmonic modes.

Both the anti-crossing of the resonant wavelengths and crossing of Q factors indicate strong mode coupling between photonic modes and plasmonic modes. To further study field distributions of the supermodes, the anti-crossing curves of their resonant wavelengths surrounded with dashed box in Fig. 2(a) are specifically illustrated in Fig. 3. The insets are their typical field distributions of TM2/EX-SPPs coupled supermodes at three different thicknesses of silica wall. As shown in Fig. 3, a pair of dispersion curves is produced due to TM2/EX-SPPs mode coupling in the coupling range, and the supermode fields are the field combinations of EX-SPPs plasmonic mode and TM2 photonic mode. But the supermode on each branch has totally different mode distributions from each other. The field on the top branch is a symmetric supermode, and will evolve from a plasmonic-like mode to a photonic-like mode; while the field on the bottom branch is an asymmetric supermode, and will evolve from a photonic-like mode to a plasmonic-like mode when silica wall thickness increases. When $d = 2.5\,\mu$m, the effective mode indices difference of two supermodes is about 0.0063, so the coupling coefficient between TM2 mode and EX-SPPs mode in this MCM is derived as $|\kappa| = 2.6 \times 10^3\ \ \mu\text{m}^{-1}$ [21]. Also two supermodes at $d = 2.5\,\mu$m have nearly equal energy distribution in silica wall and outside of outer metal film. So far we have manifested that the 2nd order coupled modes in MCM are high Q factor hybrid plasmonic/photonic modes, and could be used in many important applications requiring both high Q factor and high field enhancement factor.

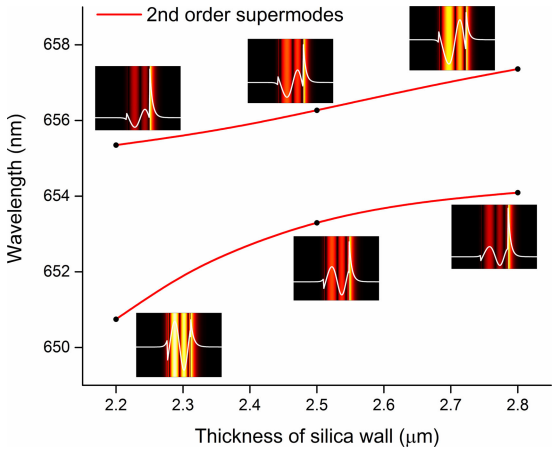

Fig. 3. Anticrossing dispersion curves of the TM2/EX-SPPs coupled supermodes. The insets are field distributions and overlaid radial amplitude distributions (white line) of second-order supermodes at different thicknesses of silica wall.

The field evolution/transition of the supermode in Fig. 3 can be interpreted by the effective potential approach. The effective potential approach provides good physical insight into many properties of the eigenmodes of optical resonance that appear as quasibound states of light [14], [22]. We write radial wave equation in a non-standard form similar to Schrödinger equation as: $\nabla_r^2\psi(r) + V_{eff}\ (r)\psi(r) = E\psi(r)$, where $E = k^2$ is the total energy and $\psi(r)$ is a position probability function of a photon [23]. The effective potential is given by $V_{eff}(r) = k^2[1 - \varepsilon(r)] + (M/r)^2 = k^2[1 - \varepsilon(r) + (n_{eff}R/r)^2]$, where $\varepsilon(r)$ is the permittivity distribution along radial direction, M is azimuthal mode number, and n_{eff} is the effective index of resonant mode. We plot the effective potential functions $V_{eff}(r)/k^2$ (azimuthal mode number $M = 956$) and field intensity distributions along the radial direction of TM2/EX-SPPs coupled modes at different wall thicknesses d of the MCM in Fig. 4. As shown in Fig. 4, the field of symmetric mode (left column) transfers from interior of silica wall to outside of outer metal film when wall thickness decreases from (a) $d = 2.8\,\mu$m to (b) $d = 2.5\,\mu$m and (c) $d = 2.2\,\mu$m. In contrast, the field of asymmetric mode (right column) transfers from outside of outer metal film to interior of silica wall when wall thickness decreases from (d) $d = 2.8\,\mu$m to (e) $d = 2.5\,\mu$m and (f) $d = 2.2\,\mu$m. For the symmetric mode, it is a photonic-like mode at $d = 2.8\,\mu$m, photons mainly concentrate inside silica wall. With the decrease of d, both the total energy and kinetic energy of confined photons in silica wall become higher [20], more photons can tunnel out through the potential barrier of outer metal film. Eventually it evolves to a plasmonic-like mode at $d = 2.2\,\mu$m. But for the asymmetric mode, it has opposite transition to the symmetric mode. It is a plasmonic-like mode at $d = 2.8\,\mu$m, and its photons mainly concentrate on outer surface of outer metal film. Because the kinetic energy of confined SPP photons becomes larger with the decrease of d, photons will tunnel into silica wall with lower potential well. So it evolves to a photonic-like mode at $d = 2.2\,\mu$m eventually.

We have studied the hybrid coupled mode between one photonic mode and one plasmonic mode on either metal film in MCM cavity. Now we explore tunable double anti-crossing or high order mode coupling between two SPPs modes and one TM mode in a single MCM cavity. Double anti-crossing phenomenon has been observed in a few photonic molecule systems, which needs some rigidly customized cavities and/or precise temperature controls [24]. However, double anti-crossing effect has not been reported so far in a single microcavity. In our calculation, double anti-crossing effect is observed in a single resonator for the first time. As shown in Fig. 2(a), strong mode anti-crossing has been generated between EX-SPPs mode and TM2 mode when d was around 2.5 μm. To achieve double anti-crossing, we fix d at 2.5 μm and then change the refractive index of inner surrounding medium, such as liquid core, from 1.33 to 1.42. The resonant wavelength and Q factor

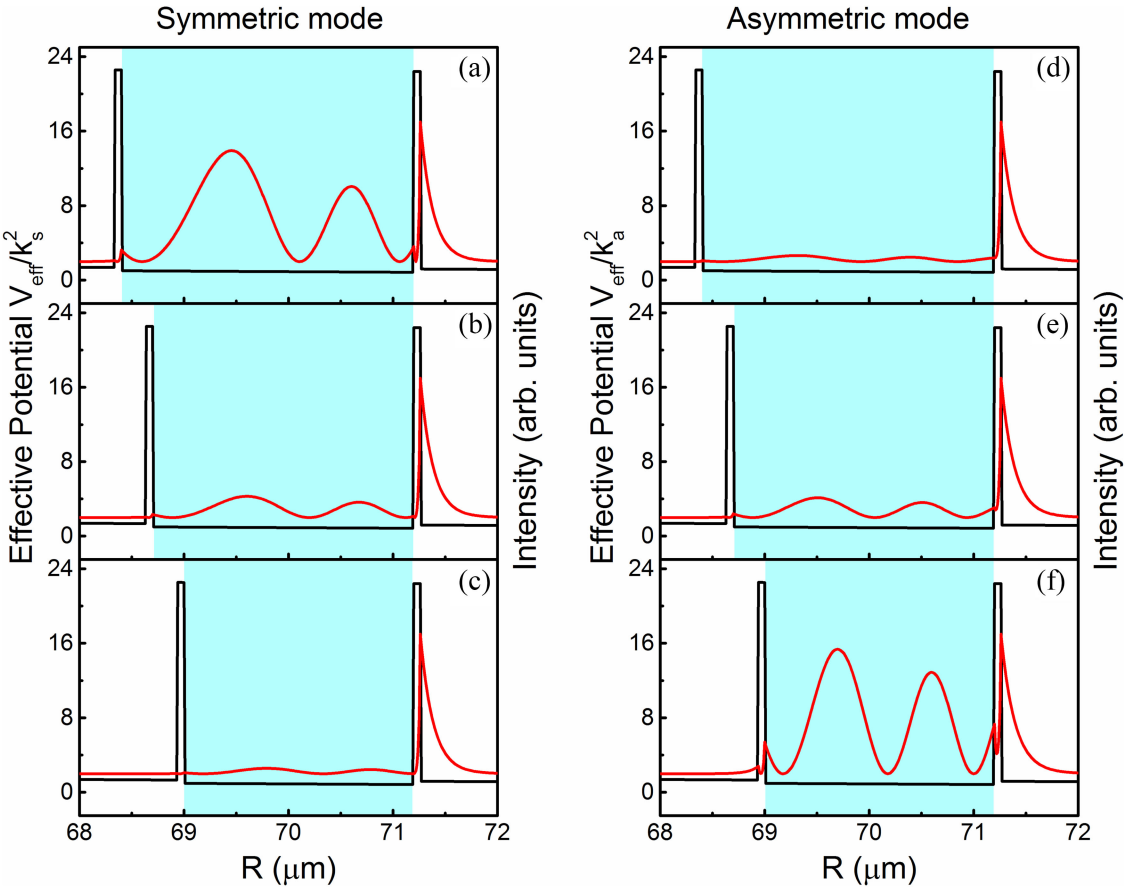

Fig. 4. Effective potential functions $V_{\text{eff}}(r)/k^2$ (black line, azimuthal mode number $M = 956$) and field intensity distributions (red line) of TM2/EX-SPPs coupled symmetric supermodes (left column) and asymmetric supermodes (right column). The silica wall thicknesses of the cavities in (a) and (d) are the same 2.8 μm, (b) and (e) 2.5 μm, and (c) and (f) 2.2 μm, respectively.

dependences on inner core index are calculated in Fig. 5. As shown in Fig. 5(a), outside of coupling range, the resonant wavelengths of TM1 mode (blue line), TM3 mode (violet line) and TM2/EX-SPPs supermodes (red line) keep almost constant when the refractive index of liquid core is changed. That is, the resonant wavelengths of these modes are almost insensitive to a change of core index because their fields hardly penetrate into core medium, as shown in Fig. 3 or Fig. 1. But the resonant wavelength of IN-SPPs mode increases almost linearly with core index because most of its energy is in the liquid core, as shown in Fig. 1(f). Therefore, through changing the core index to around 1.381, when IN-SPPs, TM2 and EX-SPPs modes have approximately equal resonant wavelengths, double anti-crossing can be formed in a single MCM cavity, which is highlighted with pink lines in Fig. 5(a). Compared to other high order coupling methods, our MCM method is not only very simple but easily tunable, which is more advantageous than other methods. In Fig. 5(b), there are two crossings at $n_{\text{in}} \sim 1.378$ and ~ 1.384 in the Q factor curves of supermodes, indicating this mode coupling is truly the double anti-crossing. Compared to single anti-crossing, double anti-crossing has lower Q factor because of additional loss of IN-SPPs mode, but still higher than pure SPPs mode. When n_{in} is around 1.381, one supermode has the lowest Q factor because it is almost the pure hybrid plasmonic mode, which will be discussed in Fig. 6.

Besides, as shown in Fig. 5, tunable mode coupling between IN-SPPs mode and photonic mode can be realized through changing the core index of MCM. For example, IN-SPPs mode can couple with TM3 and TM1 modes at the core index of around 1.35 and 1.41, respectively. And their Q factor

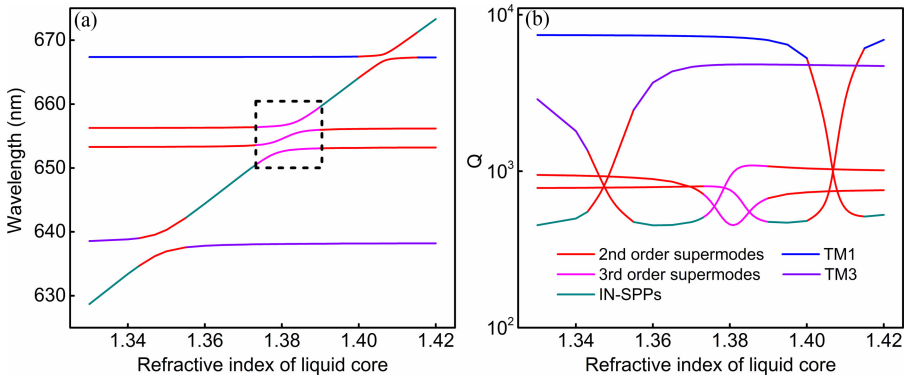

Fig. 5. (a) Resonant wavelength and (b) Q factor dependences of resonant modes (azimuthal mode number $M = 956$) on the core index of MCM.

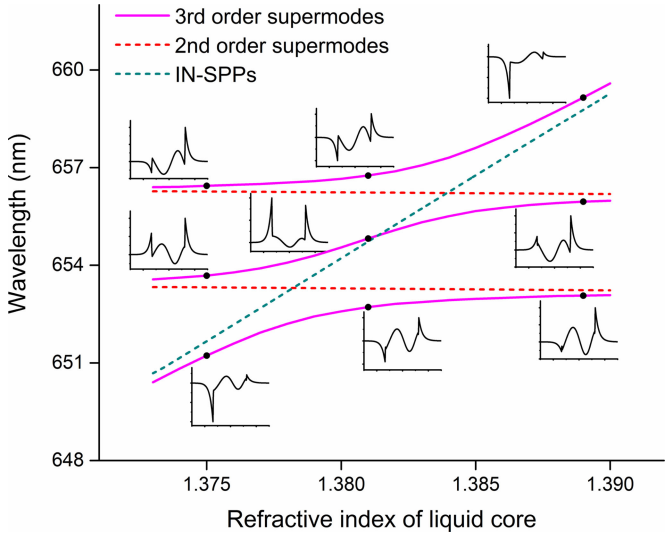

Fig. 6. Double anticrossing dispersion curves of the IN-SPPs/TM2/EX-SPPs coupled third-order supermodes. The insets are amplitude distributions of third-order supermodes at different indices of liquid core.

curves verify such the mode coupling. This mode coupling has been investigated comprehensively above, so we will not detail it again.

Finally the field distributions of double anti-crossing coupling in the dashed box of Fig. 5(a) are calculated in Fig. 6. This coupling can be regarded as the coupling between IN-SPPs mode and EX-SPPs/TM2 supermode, but is essentially the mutual coupling between three modes of IN-SPPs, TM2 and EX-SPPs modes. The generated coupled mode is hybrid plasmonic/photonic/plasmonic mode or 3rd order supermode, involving two plasmonic modes and one photonic mode. Due to double anti-crossing, there are three branches of dispersion curves for this high order supermode. These three branches have different field distributions. As shown in Fig. 6, the top branch is mainly the coupled mode between a symmetric TM2/EX-SPPs supermode and IN-SPPs mode, and its mode evolves from a symmetric TM2/EX-SPPs supermode to an IN-SPPs mode with the increase of MCM core index. Similar to the top branch, the bottom branch is the coupled mode between an asymmetric TM2/EX-SPPs supermode and an IN-SPPs mode, and its mode evolves from an IN-SPPs mode to an asymmetric TM2/EX-SPPs supermode with the increase of core index. But different to the top and bottom branches, the middle branch is the coupled mode between an asymmetric TM2/EX-SPPs supermode and an IN-SPPs mode with core index lower than 1.378,

then between a symmetric, an asymmetric supermode and an IN-SPPs modes within core index range (1.378, 1.384), and finally between a symmetric TM2/EX-SPPs supermode and IN-SPPs mode with core index larger than 1.384. These field evolutions of 3rd order supermodes can also be interpreted by the effective potential approach above. Especially, at $n_{in} \sim 1.381$, the supermode on the middle branch distributes almost all its energy on both SPPs modes, no energy on TM2 mode, so it has the lowest Q factor as the same as the pure SPP mode, as illustrated in Fig. 5(b).

Tunable double anti-crossing can also be formed by changing outer media index n_{out}. For example, if we fix d at 2.2 μm and n_{in} at 1.33, then reduce n_{out} to around 1.286, double anti-crossing phenomenon can also be observed in the proposed MCM. Further, when we increase n_{in} and n_{out} simultaneously, resonant wavelength of double anti-crossing coupling could red shift over a free spectral range. So tunable double anti-crossing at any wavelength could be expected in the MCM. Moreover, multiple anti-crossing may be expected in a single MCM composed of multiple layers of metal film. Such the coupled mode is the high Q factor hybrid plasmonic-photonic mode, possessing both high Q factor and high field enhancement factor, and will find many important applications, such as biochemical sensor.

4. Conclusion

In summary, we have studied mode couplings between plasmonic and photonic modes in a novel MCM plasmonic microcavity. Through the calculations of the dispersion relations, Q factors and field distributions, different types of mode coupling can be observed in the proposed MCM cavity. Besides the traditional mode coupling between one plasmonic mode and one photonic mode, tunable double anti-crossing coupling between two plasmonic modes and one photonic mode is formed for the first time in a single cavity. The coupled mode is the high Q factor hybrid plasmonic/photonic mode, which may find the applications requiring both high Q factor and high field enhancement, such as biochemical sensing.

References

[1] K. J. Vahala, "Optical microcavities," *Nature*, vol. 424, no. 6950, pp. 839–846, 2003.
[2] A. B. Matsko and V. S. Ilchenko, "Optical resonators with whispering-gallery modes—Part I: Basics," *IEEE J. Sel. Topics Quantum Electron.*, vol. 12, no. 1, pp. 3–14, Jan./Feb. 2006.
[3] V. S. Ilchenko and A. B. Matsko, "Optical resonators with whispering-gallery modes—Part II: Applications," *IEEE J. Sel. Topics Quantum Electron.*, vol. 12, no. 1, pp. 15–32, Jan./Feb. 2006.
[4] J. Ward and O. Benson, "WGM microresonators: Sensing, lasing and fundamental optics with microspheres," *Laser Photon. Rev.*, vol. 5, no. 4, pp. 553–570, 2011.
[5] S. Spillane, T. Kippenberg, and K. Vahala, "Ultralow-threshold Raman laser using a spherical dielectric microcavity," *Nature*, vol. 415, no. 6872, pp. 621–623, 2002.
[6] X. Fan, I. M. White, H. Zhu, J. D. Suter, and H. Oveys, "Overview of novel integrated optical ring resonator bio/chemical sensors," *Proc. SPIE*, vol. 6452, 2007, Art. no. 64520M.
[7] D. Armani, T. Kippenberg, S. Spillane, and K. Vahala, "Ultra-high-Q toroid microcavity on a chip," *Nature*, vol. 421, no. 6926, pp. 925–928, 2003.
[8] X. Yu, E. Arbabi, L. L. Goddard, X. Li, and X. Chen, "Monolithically integrated self-rolled-up microtube-based vertical coupler for three-dimensional photonic integration," *Appl. Phys. Lett.*, vol. 107, 2015, Art. no. 031102.
[9] M. Kuttge, F. J. García de Abajo, and A. Polman, "Ultrasmall mode volume plasmonic nanodisk resonators," *Nano Lett.*, vol. 10, no. 5, pp. 1537–1541, 2010.
[10] S. I. Bozhevolnyi, V. S. Volkov, E. Devaux, J.-Y. Laluet, and T. W. Ebbesen, "Channel plasmon subwavelength waveguide components including interferometers and ring resonators," *Nature*, vol. 440, no. 7083, pp. 508–511, 2006.
[11] B. Min *et al.*, "High-Q surface-plasmon-polariton whispering-gallery microcavity," *Nature*, vol. 457, no. 7228, pp. 455–458, 2009.
[12] A. Rottler, M. Harland, M. Bröll, M. Klingbeil, J. Ehlermann, and S. Mendach, "High-Q hybrid plasmon-photon modes in a bottle resonator realized with a silver-coated glass fiber with a varying diameter," *Phys. Rev. Lett.,* vol. 111, 2013, Art. no. 253901.
[13] J. Gu, Z. Zhang, M. Li, and Y. Song, "Mode characteristics of metal-coated microcavity," *Phys. Rev. A*, vol. 90, 2014, Art. no. 013816.
[14] Y.-F. Xiao *et al.*, "High-Q exterior whispering-gallery modes in a metal-coated microresonator," *Phys. Rev. Lett.*, vol. 105, 2010, Art. no. 153902.

[15] S. Cai, Y. Xiang, Y. Miao, M. Li, Y. Peng, and Y. Song, "Mode coupling in metal-coated microsphere," *Opt. Exp.*, vol. 24, no. 13, pp. 13832–13838, 2016.
[16] Q. Lu *et al.*, "Strong coupling of hybrid and plasmonic resonances in liquid core plasmonic micro-bubble cavities," *Opt. Lett.*, vol. 40, no. 24, pp. 5842–5845, 2015.
[17] I. Malitson, "Interspecimen comparison of the refractive index of fused silica," *J. Opt. Soc. Amer.*, vol. 55, no. 10, pp. 1205–1209, 1965.
[18] P. B. Johnson and R.-W. Christy, "Optical constants of the noble metals," *Phys. Rev. B*, vol. 6, no. 12, 1972, Art. no. 4370.
[19] M. Oxborrow, "Traceable 2-D finite-element simulation of the whispering-gallery modes of axisymmetric electromagnetic resonators," *IEEE Trans Microw. Theory Techn.*, vol. 55, no. 6, pp. 1209–1218, Jun. 2007.
[20] Y. Yin *et al.*, "Hybridization of photon-plasmon modes in metal-coated microtubular cavities," *Phys. Rev. A*, vol. 94, 2016, Art. no. 013832.
[21] H. A. Haus, *Waves and Fields in Optoelectronics.* Englewood Cliffs, NJ, USA: Prentice-Hall, 1984.
[22] B. Johnson, "Theory of morphology-dependent resonances: Shape resonances and width formulas," *J. Opt. Soc. Amer. A*, vol. 10, no. 2, pp. 343–352, 1993.
[23] M. I. Cheema and A. G. Kirk, "Accurate determination of the quality factor and tunneling distance of axisymmetric resonators for biosensing applications," *Opt. Exp.*, vol. 21, no. 7, pp. 8724–8735, 2013.
[24] C. Yang *et al.*, "Realization of controllable photonic molecule based on three ultrahigh-Q microtoroid cavities," *Laser Photon. Rev.*, vol. 11, no. 2, 2017, Art. no. 1770021.